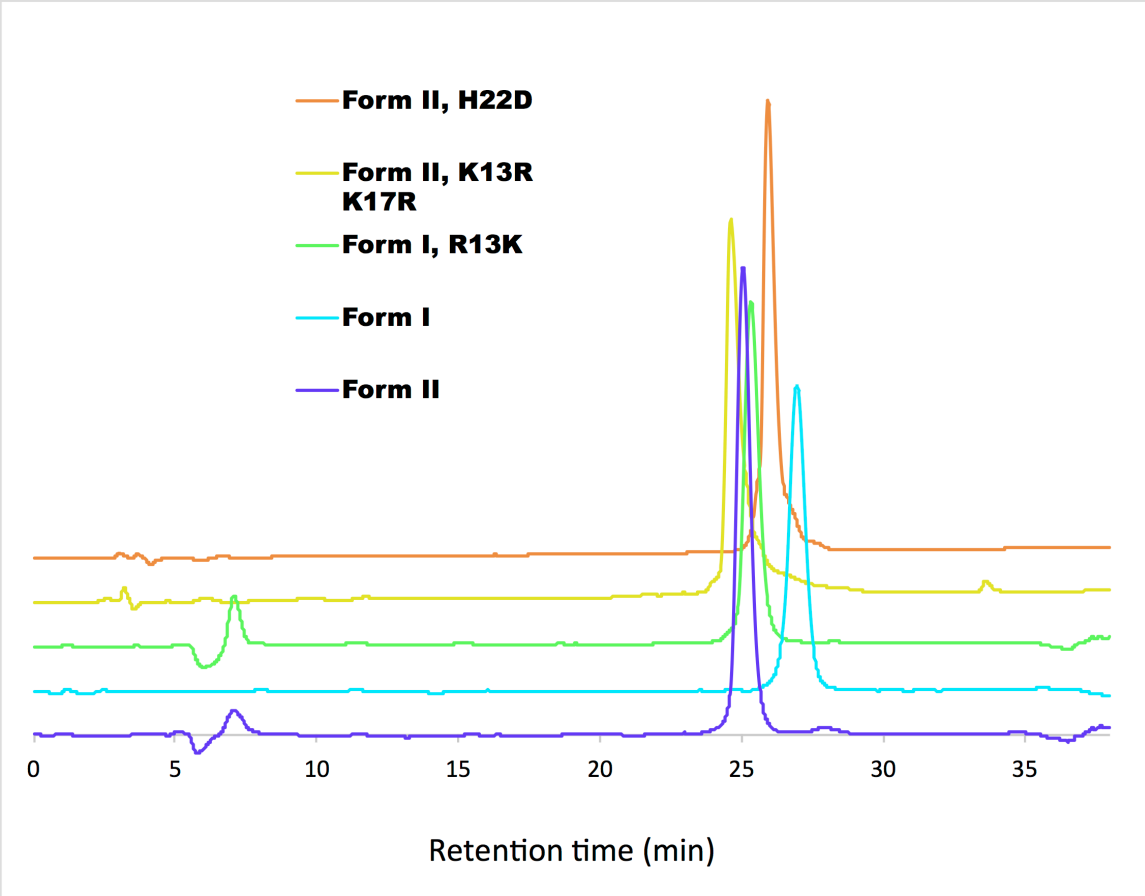

Supplementary Figure 1

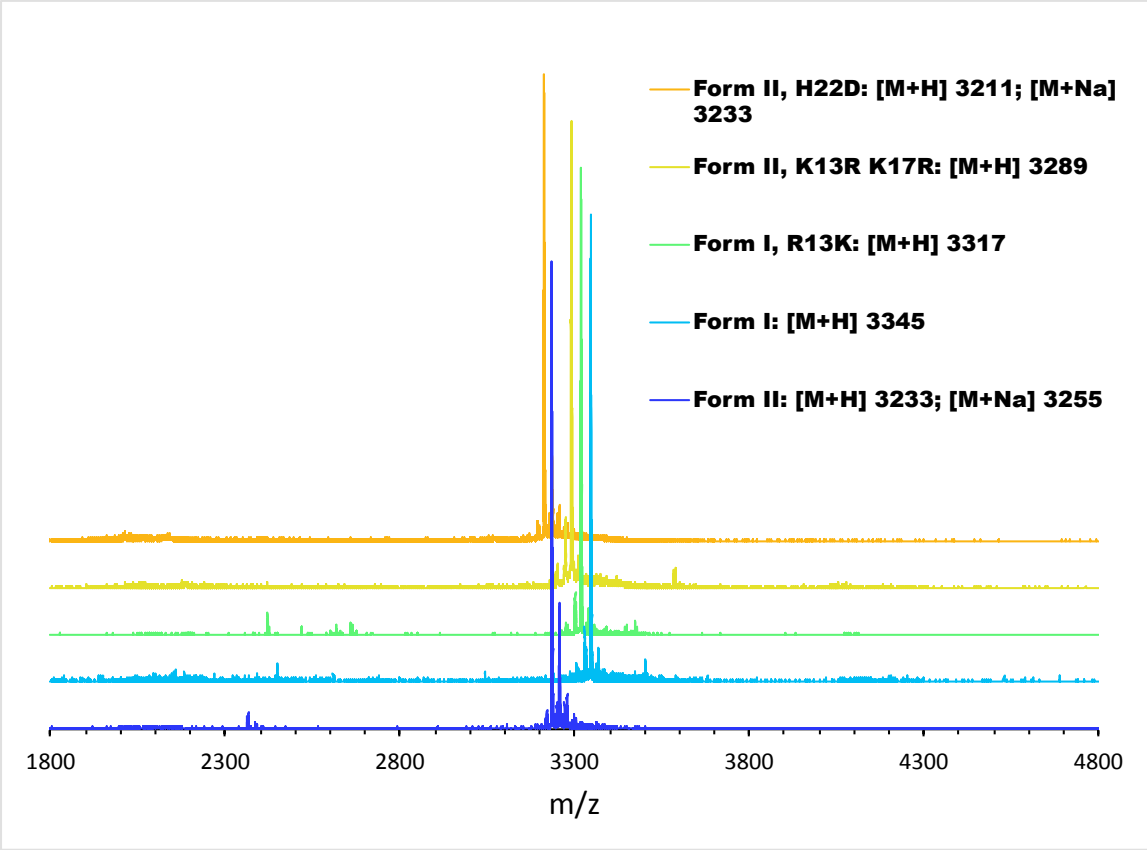

Supplementary Figure 2

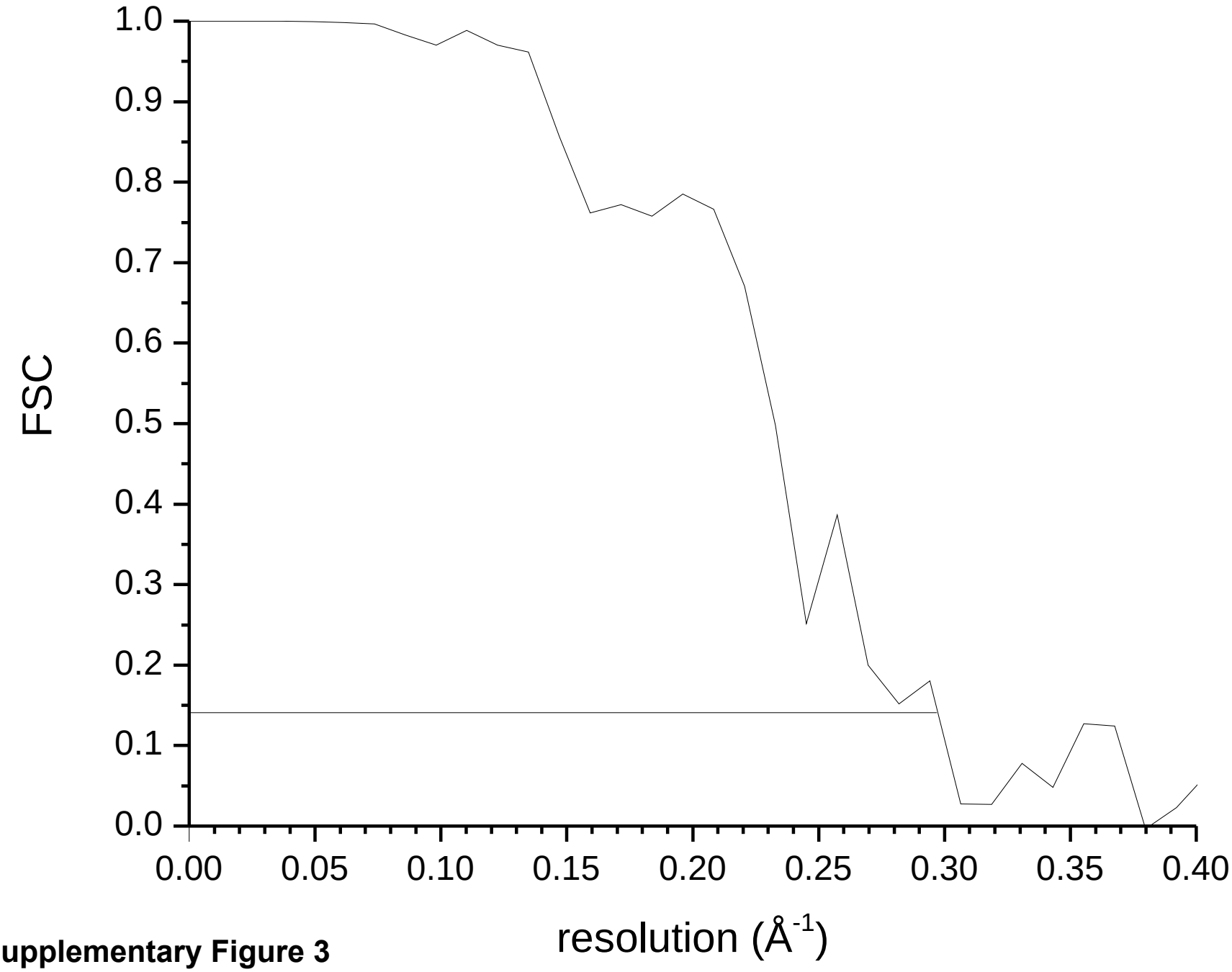

Supplementary Figure 3

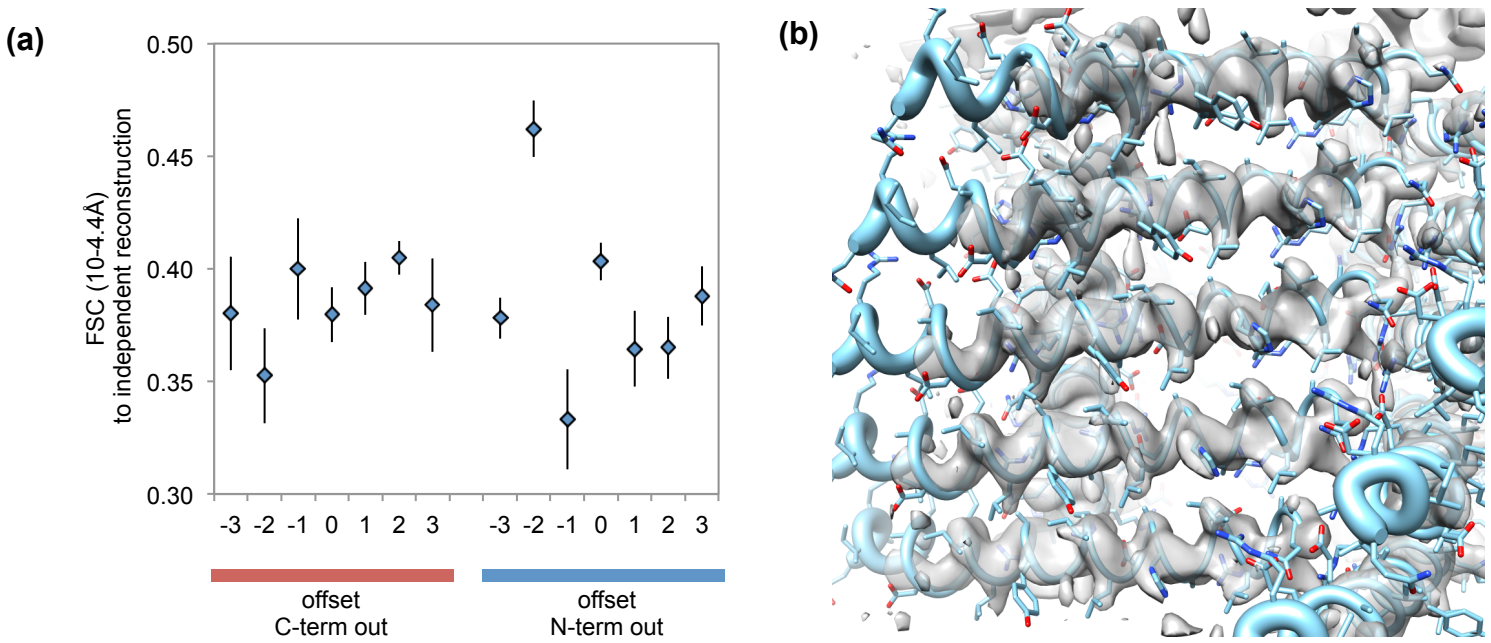

Supplementary Figure 4

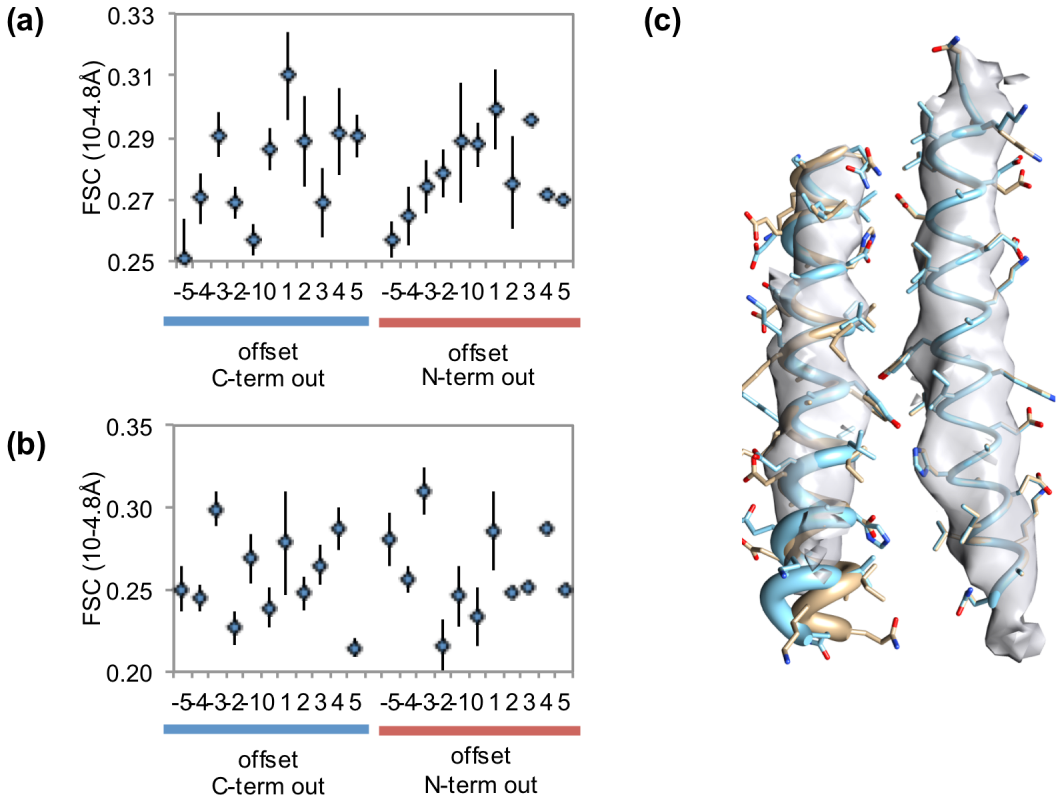

Supplementary Figure 5

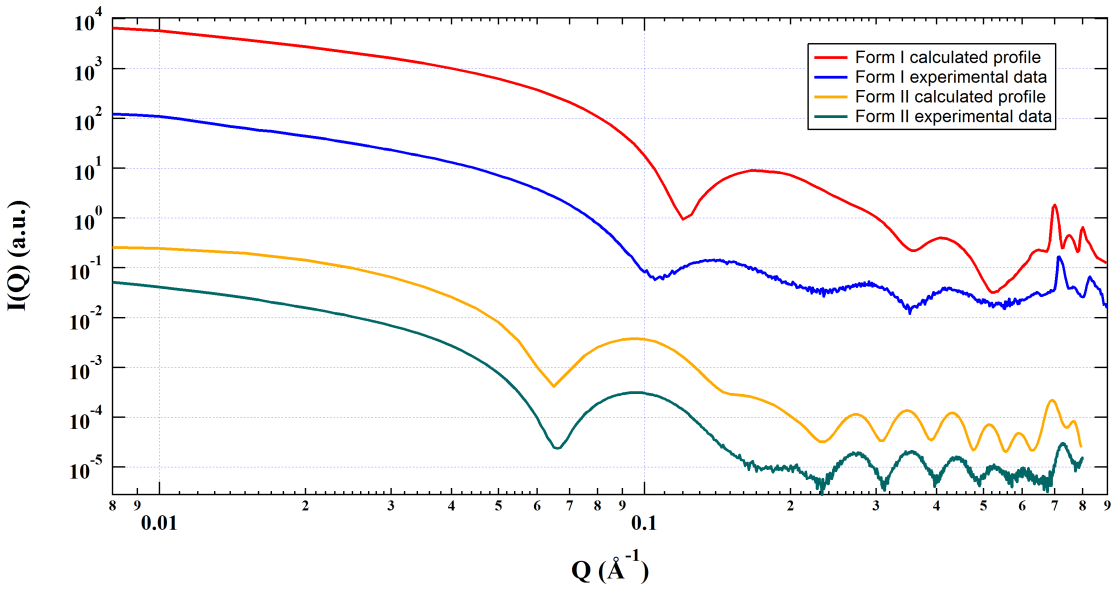

Supplementary Figure 6

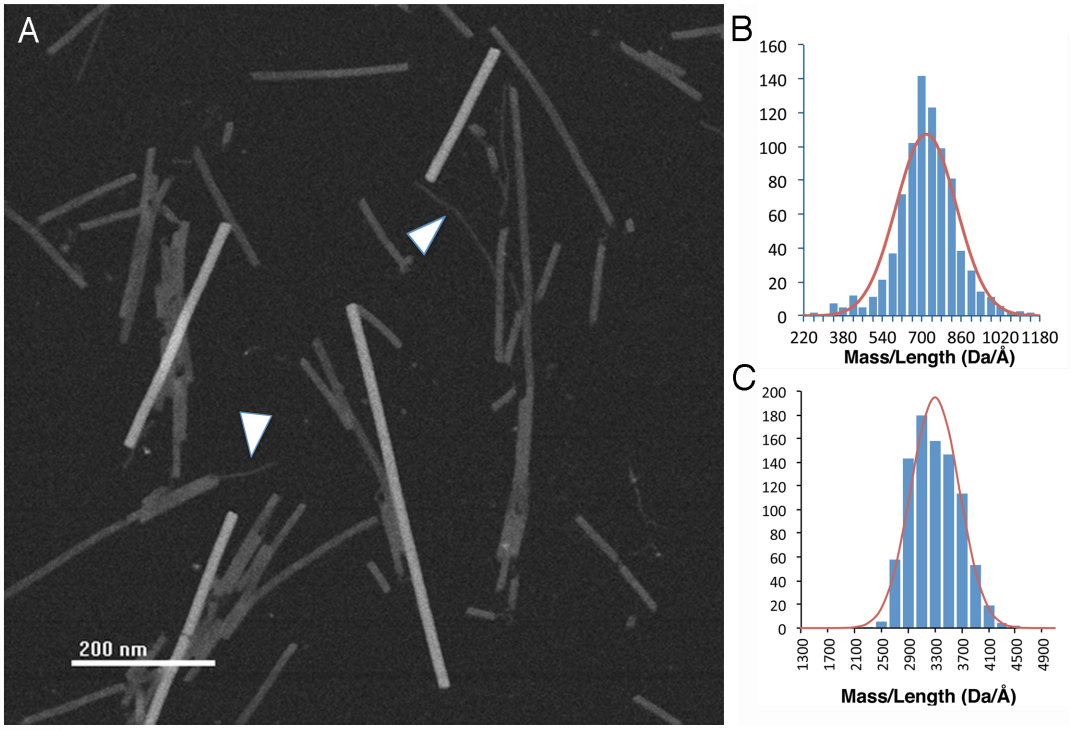

Supplementary Figure 7

Supplementary Figures and Movies

Supplementary Figure 1, related to Experimental Procedures) Analytical reverse phase HPLC traces of purified peptide specimens.

Supplementary Figure 2, related to Experimental Procedures) MALDI-TOF mass spectra of purified peptides.

Supplementary Figure 3, related to Experimental Procedures) An FSC curve for the Form I filaments generated using two completely independent (non-overlapping) data sets. Using the FSC=0.143 criterion (Rosenthal and Henderson, 2003) an overly optimistic resolution of 3.3 Å resolution is achieved.

Supplementary Figure 4, related to Experimental Procedures) (a) An evaluation of the agreement of 14 threadings of Form I models against an independent map reconstruction from half the images (not used for refinement) yields a clear signal for the correct configuration of the model. (b) The resulting refined model (after an additional round of refinement against a reconstruction using the full dataset) shows good agreement with sidechain density. The thickness of the backbone indicates real-space refined B-factors, identifying regions of local heterogeneity of the assembly

Supplementary Figure 5, related to Experimental Procedures) An evaluation of the agreement of (a) 22 threadings of the inner wall of Form II models and (b) 22 threadings of the outer wall of the Form II assembly against an independent map

reconstruction. These yield a clear signal for the correct configuration of the inner wall, but two equally good configurations of the outer wall. (c) A superposition of these two configurations show that the outer wall models only differ in their polarity; the nearly-palindromic sequence makes disambiguation of the two configurations challenging. The thickness of the backbone indicates real-space refined B factors, identifying regions of local heterogeneity of the assembly.

Supplementary Figure 6, related to Experimental Procedures) Experimental SAXS/WAXS scattering profile for the Form I and Form II assemblies (4 mg/mL) in acetate buffer (10 mM, pH 4.0) along with simulated data calculated using Crysol for structural models corresponding to those derived from the respective peptides using cryo-EM helical reconstruction.

Supplementary Figure 7, related to Experimental Procedures) Bright-field STEM analysis of freeze-dried specimens of assemblies derived from the Form II peptide (0.3 mg/mL) in acetate buffer (10 mM, pH 4.0). (a) Representative STEM image of the Form II assemblies. The arrowheads indicate the positions of several thin fibers (4.3 nm in diamater) that are observed to emerge from the ends of the larger Form II nanotubes. TMV was employed as a calibrant for the mass-per-length measurements and can be observed as the larger diameter assemblies within the image. (b) Histogram from experimental mass-per-length measurements on the thin fibrils. The experimentally determined mass-per-length value of 718 ± 61 Dalton/Å compares well to that of 719 Dalton/Å calculated for a fiber based on a helical

bilayer ((2 x 3234 Da)/9.0 Å helix-helix distance). (c) Histogram from experimental mass-per-length measurements on the Form II nanotubes. The experimentally determined mass-per-length value of 3300 ± 181 Da/Å compares well with the calculated value of 3080 Da/Å from the structural model of the Form II nanotube ((2 x 3234 Da)/2.1 Å axial rise per asymmetric unit).

Supplementary Movie 1, related to Figure 3) This animation shows averaged power spectra from two different twist bins of the Form I filaments which behave exactly as expected from the sorting in Fig. 3a: the twist of the long-pitch 4-start helices is variable (red arrow, n=4), while the stacking of helices on top of each other is fairly fixed (blue and yellow arrows). The yellow arrow points to the 1/(7.9 Ångstrom) layer line (n=3), while the blue arrow points to the 1/(9.0 Å) layer line (n=-1).

Supplementary Movie 2, related to Figure 3) As with the Form I filaments in Supp. Movie 1, the Form II filament sorting (Fig. 3b) is validated by comparing averaged power spectra from two different twist bins. The variability of the long-pitch helices (near-equatorial layer line) is consistent with the histogram in Fig. 3b.

Reference

Rosenthal, P.B., and Henderson, R. (2003). Optimal Determination of Particle Orientation, Absolute Hand, and Contrast Loss in Single-particle Electron Cryomicroscopy. Journal of Molecular Biology *333*, 721-745.